

Evidence for weak antilocalization-weak localization crossover and metal-insulator transition in $\text{CaCu}_3\text{Ru}_4\text{O}_{12}$ thin films

Subhadip Jana,^{1,2,*} Shwetha G.Bhat,³ B.C.Behera,¹ L.Patra,⁴ P.S.Anil Kumar,³ B.R.K.Nanda,⁴ and D.Samal^{1,2}

¹*Institute of Physics, Sachivalaya Marg, Bhubaneswar-751005, India*

²*Homi Bhabha National Institute, AnushaktiNagar, Mumbai-400085, India*

³*Department of Physics, Indian Institute of Science Bangalore-560012, India*

⁴*Condensed Matter Theory and Computational Lab,*

Department of Physics, Indian Institute of Technology, Madras, India

Artificial confinement of electrons by tailoring the layer thickness has turned out to be a powerful tool to harness control over competing phases in nano-layers of complex oxides. We investigate the effect of dimensionality on transport properties of d -electron based heavy-fermion metal $\text{CaCu}_3\text{Ru}_4\text{O}_{12}$. Transport behavior evolves from metallic to localized regime upon reducing thickness and a metal insulator transition is observed below 3 nm film thickness for which sheet resistance crosses $h/e^2 \sim 25 \text{ k}\Omega$, the quantum resistance in 2D. Magnetotransport study reveals a strong interplay between inelastic and spin-orbit scattering lengths upon reducing thickness, which results in weak antilocalization (WAL) to weak localization (WL) crossover in magnetoconductance.

I. INTRODUCTION

Reducing the dimensionality of a system often engenders electromagnetic properties sharply different from their bulk counterpart. It mainly arises due to enhanced quantum effects and increased correlations due to reduction in available phase space and screening¹. The interplay between electron band width (W) and onsite Coulomb energy (U) in correlated electron system sensitively depends on the lattice dimensionality of the electron system. Manipulation of correlated electronic states in artificial crystal structures by exploiting their layer thickness down to unit cell level and epitaxial strain (without resorting to any chemical substitution that might induce unintentional disorder) is seen as a viable route to obtain more insight into these materials and renders a perfect platform to search for unforeseeable complex phenomena²⁻⁷. Besides U and W , spin-orbit interaction plays a significant role in governing the underlying electronic properties as evidenced in the study of Ir based oxides⁸⁻¹².

Conducting systems with strong spin-orbit coupling (SOC) often manifest weak antilocalization (WAL) effect and has extensively been explored in materials containing heavy elements (like Bi,Ir,Pt,Au)¹³⁻¹⁵. Besides, Dresselhaus/ Rashba type SOC effects in systems that lack bulk inversion symmetry/asymmetry in confining potential (for e.g. modulation doped semiconductor heterostructure $\text{GaAs}/\text{Al}_x\text{Ga}_{1-x}\text{As}$, and $\text{LaAlO}_3/\text{SrTiO}_3$) has triggered diverse research¹⁶⁻¹⁹. It is observed that applying an electric field across interface in the above cases induces WAL-WL crossover. In present study, we demonstrate a possibility for WAL-WL crossover by systematically manipulating layer thickness in heavy fermionic $\text{CaCu}_3\text{Ru}_4\text{O}_{12}$ (CCRO) system with cubic symmetry (space group Im-3).

Layered ruthenates with different dimensionality, so called nature's engineered Ruddlesden-Popper (RP) type phases have attracted significant attention since they ex-

hibit unique electronic and magnetic ground states such as unconventional spin-triplet superconductivity, metamagnetism and electron nematic phase, highly conducting ferromagnetism and spin glass behaviour^{6,20-22}. The interplay among electron correlation, spin orbit interaction and dimensionality makes ruthenates more promising and a small perturbation can readily tip the balance and promote unexpected changes in the electronic property. CCRO is intriguingly debated as a rare class of d electron based heavy-fermion metal with excellent metallic conductivity along with a signature for broad hump in magnetic susceptibility around 150-200K²³⁻²⁶. If the heavy fermionic metals can be made 2D, unprecedented quantum phenomena are expected to result, and such studies are very much desirable.

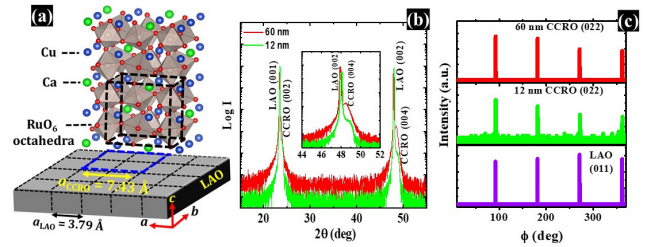


FIG. 1. (a) Schematic structure of CCRO on LAO. (b) $2\theta - \theta$ XRD pattern for (001) oriented CCRO film on LAO (001) of 12 nm and 60 nm thick films. (c) ϕ scan about (011) of LAO and (022) of CCRO films (60 nm and 12 nm) showing the epitaxial relation.

We fabricate single-crystalline epitaxial CCRO thin films of varying layer thickness and investigate the dimensional effect on its magnetotransport properties. We observe that upon reduction of CCRO thickness, transport behavior evolves from metallic to localized regime and a thickness driven metal insulator transition (MIT) is observed below 3 nm for which the room temperature sheet resistance crosses $h/e^2 \sim 25 \text{ k}\Omega$, the quantum

resistance in 2D²⁷. More importantly, from magnetoconductance we observe a strong interplay among inelastic (L_{Th}) and spin-orbit (l_{so}) scattering lengths that gives rise to weak antilocalization (WAL) - weak localization (WL) crossover upon reducing thickness. Using 2D magnetotransport theory and magnetotransport measurement, we elucidate the evolution of different types of scattering process (i.e. spin-orbit, phase breaking) with variation of thickness.

II. THIN FILM GROWTH AND STRUCTURAL CHARACTERIZATION

A series of high-quality single-crystalline epitaxial CCRO films with varying thickness were grown on LaAlO_3 (001) substrates ($a = 3.79 \text{ \AA}$) using pulsed laser deposition (PLD) with a KrF excimer laser ($\lambda = 248 \text{ nm}$). The polycrystalline CCRO PLD-target material was prepared by stoichiometrically mixing CaCO_3 , CuO , RuO_2 and heating the mixture for 26 hours at $1050 \text{ }^\circ\text{C}$ temperature in open air and under ambient pressure²⁵. Single phase was obtained after many cycles of heating and grinding. During thin film growth, the substrate temperature and the O_2 partial pressure was maintained at $650 \text{ }^\circ\text{C}$ and $5 \times 10^{-3} \text{ mbar}$ respectively and the deposition was carried out with a laser fluence $\sim 3 \text{ J/cm}^2$. Before the deposition, target was pre-ablated for 2 minutes to remove any possible surface contamination. The structural details of the films were characterized by X-ray diffraction (XRD) scan (using Rigaku Smart-Lab X-ray diffractometer in parallel-beam geometry with high resolution of Cu-K_α radiation). The thicknesses of the films were calibrated with the number of laser pulses using cross-sectional SEM. Bulk CCRO exhibits cubic symmetry (Im-3 space group (No: 204)) with a lattice parameter of 7.43 \AA ²⁵ which is close to twice the lattice parameter of LaAlO_3 (LAO) (Fig. 1(a)). Thus, one can expect an in-plane tensile strain of $+1.97\%$ for CCRO films with a cube-on-cube epitaxy on LAO. Fig. 1(b) exhibits wide-angle diffraction pattern for representative 60 nm and 12 nm thickness of CCRO films, indicating a c-axis oriented growth. The inset to Fig. 1(b) shows a zoom-in view of diffraction peak around (002) of LAO. It is observed that the CCRO peak is close to the substrate for 60 nm than the 12 nm, signaling a compressed out-of-plane lattice in latter case. To verify the in-plane epitaxial relationship in these films, the φ scans were performed on both 60 nm and 12 nm films about (022) plane of CCRO in the vicinity of (011) of LAO (Fig. 1(c)). Four equally spaced distinct peaks with a relative separation of 90° (four-fold symmetry) were observed, suggesting an epitaxial growth of CCRO layer on LAO i.e.: $[100] \text{ LAO} \parallel [100] \text{ CCRO}$. Altogether, our structural characterization implies an epitaxial (001) oriented growth of CCRO on LAO (001) substrate.

III. ELECTRON TRANSPORT

We investigate the electrical transport properties of CCRO films with thicknesses (t) ranging from 1.5 to 60 nm. Fig. 2(a) shows the variation of sheet resistance (R_s) as a function of temperature. For films with $t \geq 3 \text{ nm}$, R_s values are found to be below $25 \text{ k}\Omega$ ($h/e^2 \simeq 25 \text{ k}\Omega$) across the whole temperature range (2–300 K). However, the value of R_s for the thinnest film with $t = 1.5 \text{ nm}$ crosses $25 \text{ k}\Omega$ indicating a transition to insulating state. Based on Ioffe and Regel criterion, MIT is expected in the limit of $k_F l_e \simeq 1$ where k_F , l_e are Fermi wave vector and mean free path respectively²⁸ and an approximate value for the Mott-Ioffe-Regel limit in two dimensions is h/e^2 ²⁷. The systematic increase in R_s and its rise above Ioffe-Regel limit indicates the occurrence of localization effect as the thickness of CCRO film is reduced.

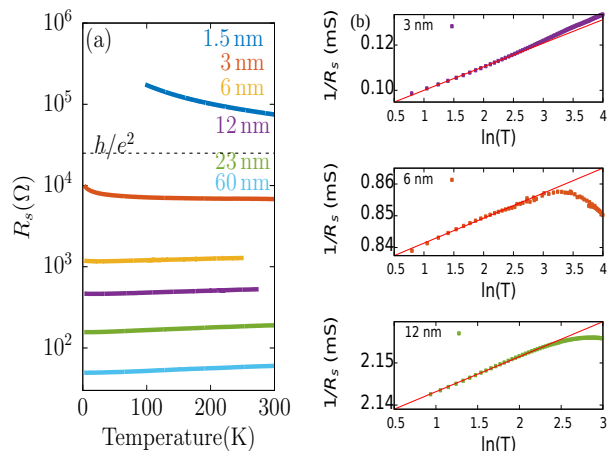


FIG. 2. (a) $R_s(T)$ for films of different thickness (MIT using Ioffe-Regel criterion is denoted by dotted line), (b) $1/R_s$ vs $\ln(T)$ plots for films of various thickness that reveals the signature for quantum interference effect in the low temperature regime.

A. Arrhenius and Variable Range Hopping behaviour

Transport in 1.5 nm film follows Arrhenius type behavior $\sigma \propto \exp(-E_g/2kT)$ and yields an activation energy gap E_g of 31 meV, which is obtained by fitting the data in the temperature range 300-160 K (Fig. 3(a)). On the contrary for the case of 3 nm film, which exhibits a negative temperature coefficient ($d\rho/dT < 0$) and is on the verge MIT, the transport behavior can be described by a variable range hopping (VRH) type of conduction. VRH conduction scenario involves hopping of electrons between the localized electronic states within narrow bands close to the Fermi energy and conductivity σ is given by $\sigma = C \exp[-(T_0/T)^\alpha]$, where T_0 depend on the density of localized states and spread of wave functions. VRH conductivity can be either of Mott or Efros-

Shklovskii (ES) type and for a two dimensional case they are characterized by the exponent $\alpha = 1/3$ and $\alpha = 1/2$ respectively^{29,30}. In our case for 3 nm CCRO film, the fit to the conductivity data in the temperature range 50 K $\leq T \leq$ 300 K (Fig. 3(b)) yields $\alpha = 0.501$ (ES type) indicating the existence of Coulomb charge gap.

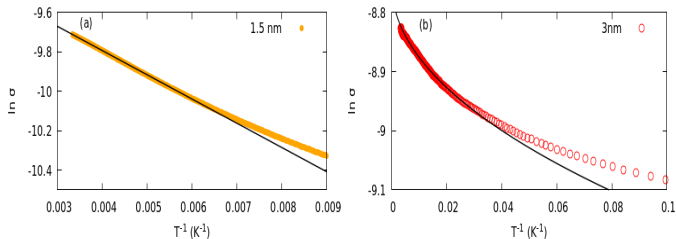


FIG. 3. (a) Resistivity fitting with Arrhenius for 1.5 nm, (b) VRH (ES type) 3 nm thick film respectively (black solid lines are theoretical expressions).

A closer inspection of R_s vs T plot on the low temperature side reveals upturn in the metallic regime (not shown here) and this could be attributed to quantum interference effect. In presence of quantum interference effect conductance shows logarithmic temperature dependence which can be expressed as (for 2D),³¹

$$\sigma(T) = \sigma_0 + \frac{pe^2}{2h\pi^2} \ln\left(\frac{T}{T_0}\right),$$

where $\sigma(T)$ is sheet conductance at temperature T , p is defined as $L_{Th} = aT^{-p/2}$ and T_0 is constant.

Fig. 2(b) shows the logarithmic temperature dependence of reciprocal sheet resistance for representative films (3, 6, 12 nm) which is fitted well in low temperature regime.

IV. MAGNETOTRANSPORT

To examine the changes in electron scattering process with the variation of film thickness, magnetotransport measurements were performed using physical property measurement system (PPMS Quantum Design) in four probe geometry, down to 2 Kelvin temperature and a magnetic field upto 8 Tesla.

Quantum interference among scattered electrons depends on their trajectory configuration. The interference correction to classical Drude conductivity tend to vanish in most cases after averaging over random scattering centers, except for the scattered electrons which propagate in identical time-reversed closed trajectories that gives rise to quantum interference correction to conductivity. Such kind of trajectories are known as ‘‘Cooperon loop’’(CL) and depending upon constructive (destructive) interference among the scattered electrons in CL, it manifests WL (WAL) effect. These quantum effects can be captured by measuring conductance in presence of magnetic field. Fig. 4(a) shows the measured out of plane magnetoconductance (MC) $\Delta\sigma$ in units of $\frac{e^2}{\pi h}$ at

2 K. Fig. 4(b),(c) shows the same after subtracting classical B^2 contribution that arises due to Lorentz force for film thicknesses ranging from 23 to 3 nm. A negative MC is observed for films with larger thickness i.e $t \geq 12$ nm. However, a crossover from negative to positive MC occurs as we reduce thickness. We attribute the positive (negative) magnetoconductance to WL (WAL) effect.

To shed light on the observed magnetoconductance crossover, we fit the magnetoconductance curves with Hikami-Larkin-Nagaoka (HLN) equation³² in 2D limit to extract the characteristic scattering lengths. For the convenience of experimental data fitting, we express extended form of HLN equation (Eq.1) in 2D limit in terms of elastic, inelastic and spin-orbit scattering lengths which are denoted as l_e , L_{Th} , l_{so} respectively (see Supplementary Material for detailed derivation).

$$\Delta\sigma(B) = -\frac{e^2}{2\pi^2\hbar} \left[\psi(1/2 + B_e/B) + \log(B/B_e) \right. \\ \left. + \frac{1}{2} \left\{ \psi(1/2 + B_{Th}/B) + \log(B/B_{Th}) \right\} \right. \\ \left. - \frac{3}{2} \left\{ \psi(1/2 + \frac{B_{Th} + B_{so}}{B}) + \log\left(\frac{B}{B_{Th} + B_{so}}\right) \right\} \right] \quad (1)$$

where $\psi(x)$ is digamma function, B is external magnetic field and B_e, B_{Th}, B_{so} are related to l_e, L_{Th}, l_{so} with following relations $B_i = \hbar/4el_i^2$ respectively. 2D limit is defined as film thickness (t) which is less than L_{Th} (where $l_i = (D\tau_i)^{1/2}$); where D is Diffusion coefficient and $D \propto v_F^2$ (v_F is Fermi velocity) and τ_i is scattering time for corresponding length.

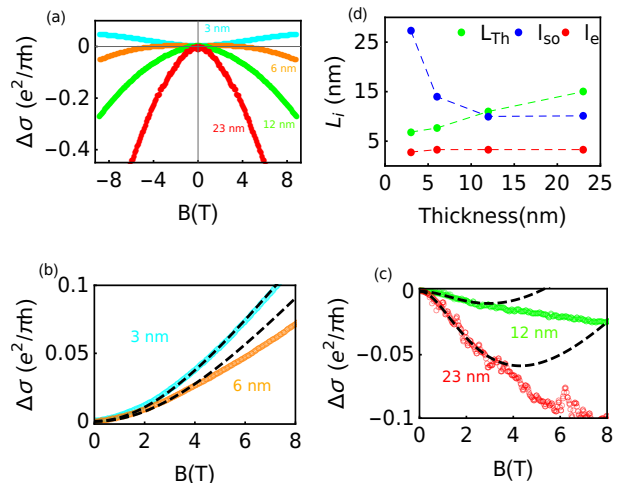


FIG. 4. (a) Magnetoconductance $\Delta\sigma = \sigma(B) - \sigma(0)$ measured for films at 2 K temperature including classical contribution ($\propto B^2$). (b),(c) Fitted with HLN equation (dashed black lines) after subtracting B^2 contribution from experimental data,¹⁴. (d) L_{Th}, l_{so}, l_e extracted from fits.

After subtraction of classical contribution to magnetoconductance $\propto B^2$ ¹⁴, $\Delta\sigma(B)$ is fitted as per Eq.(1)

which is shown in Fig. 4(b),(c). The extracted lengths from the fitting are shown in Fig. 4(d). The extracted lengths show a crossover from $L_{Th} < l_{so}$ for the films with thickness 3, 6 nm and $L_{Th} > l_{so}$ for 12, 23 nm which is consistent with WL-WAL crossover.

Below we discuss case by case study for the observed magneto conductance crossover with thickness variation. It is evident from Fig. 4(b) that 3, 6 nm thick films show WL effect (i.e $\Delta\sigma(B)$ increases with increment of magnetic field). Since $L_{Th} < l_{so}$ (for 3, 6 nm films) the spin-orbit related scattering effect becomes redundant (spin-orbit interaction strength $\propto 1/l_{so}^2$) for the phase space in which quantum coherence is maintained, electron encountering SO scattering is very weak. In other words, small L_{Th} allows CL in very short length scale where SO interaction is not able to rotate the spin and thus results in WL due to constructive interference. In WL regime, magnetic flux induces additional phase difference between two electrons moving in time-reversed identical closed trajectory and this additional phase difference breaks constructive interference and as a result conductivity increase with the application of magnetic field. For films with $t \geq 12$ nm, L_{Th} tends to increase and l_{so} gradually decreases. Therefore electrons are able to move relatively more distance by maintaining phase coherence and simultaneously due to smaller value of l_{so} , electrons encounter spin-orbit elastic scattering within a shorter distance. Therefore WAL becomes prominent

with increasing thickness and is a cumulative effect of above two factors.

V. CONCLUSION

In conclusion, we have demonstrated that epitaxial single crystalline thin films of heavy-fermion correlated metal CCRO grown on LAO can be driven to an insulating state upon reducing its thickness down to 1.5 nm. More importantly, we find that magnetoconductance shows a crossover from WAL to WL behaviour with reduction of film thickness. From analysis of magneto-transport data, we realize that a subtle interplay between effective spin-orbit scattering and inelastic scattering of electrons could render such crossover. Our study elucidates an important role of dimensionality on quantum transport behavior in CCRO.

ACKNOWLEDGEMENT

S.J and D.S acknowledge V.Tripathy, S.Mandal, D.S and B.C.B acknowledge the financial support from Max-Planck Partner Group. B.R.K.N acknowledges Department of Science and Technology, India, for Grant No-EMR/2016/003791. S.G.B would like to acknowledge INSPIRE Faculty award, DST, INDIA for the financial support. P.S.A.K acknowledges Nano Mission, DST, INDIA for funding support.

* subhadip.j@iopb.res.in

- ¹ M. Imada, A. Fujimori, and Y. Tokura, Reviews of modern physics **70**, 1039 (1998).
- ² R. Scherwitzl, S. Gariglio, M. Gabay, P. Zubko, M. Gibert, and J.-M. Triscone, Physical Review Letters **106**, 246403 (2011).
- ³ K. Yoshimatsu, T. Okabe, H. Kumigashira, S. Okamoto, S. Aizaki, A. Fujimori, and M. Oshima, Physical review letters **104**, 147601 (2010).
- ⁴ A. Boris, Y. Matiks, E. Benckiser, A. Frano, P. Popovich, V. Hinkov, P. Wochner, M. Castro-Colin, E. Detemple, V. K. Malik, *et al.*, Science **332**, 937 (2011).
- ⁵ P. King, H. Wei, Y. F. Nie, M. Uchida, C. Adamo, S. Zhu, X. He, I. Božović, D. G. Schlom, and K. M. Shen, Nature nanotechnology **9**, 443 (2014).
- ⁶ S. Stemmer and S. J. Allen, Reports on Progress in Physics **81**, 062502 (2018).
- ⁷ D. Samal, H. Tan, H. Molegraaf, B. Kuiper, W. Siemons, S. Bals, J. Verbeeck, G. Van Tendeloo, Y. Takamura, E. Arenholz, *et al.*, Physical review letters **111**, 096102 (2013).
- ⁸ P. Schütz, D. Di Sante, L. Dudy, J. Gabel, M. Stübinger, M. Kamp, Y. Huang, M. Capone, M.-A. Husanu, V. Strocov, *et al.*, Physical review letters **119**, 256404 (2017).
- ⁹ J. H. Gruenewald, J. Nichols, J. Terzic, G. Cao, J. W. Brill, and S. S. A. Seo, Journal of Materials Research **29**, 2491 (2014).
- ¹⁰ B. Kim, H. Jin, S. Moon, J.-Y. Kim, B.-G. Park, C. Leem,

- J. Yu, T. Noh, C. Kim, S.-J. Oh, *et al.*, Physical review letters **101**, 076402 (2008).
- ¹¹ J. Matsuno, K. Ihara, S. Yamamura, H. Wadati, K. Ishii, V. V. Shankar, H.-Y. Kee, and H. Takagi, Physical review letters **114**, 247209 (2015).
- ¹² J. G. Rau, E. K.-H. Lee, and H.-Y. Kee, Annual Review of Condensed Matter Physics **7**, 195 (2016).
- ¹³ A. V. Matetskiy, N. V. Denisov, A. V. Zotov, and A. A. Saranin, Nano letters **19**, 570 (2018).
- ¹⁴ M. Jenderka, J. Barzola-Quiquia, Z. Zhang, H. Frenzel, M. Grundmann, and M. Lorenz, Physical Review B **88**, 045111 (2013).
- ¹⁵ H. Beckmann, R. Schäfer, W. Li, and G. Bergmann, EPL (Europhysics Letters) **33**, 563 (1996).
- ¹⁶ W. Knap, C. Skierbiszewski, A. Zduniak, E. Litwin-Staszewska, D. Bertho, F. Kobbi, J. Robert, G. Pikus, F. Pikus, S. Iordanskii, *et al.*, Physical Review B **53**, 3912 (1996).
- ¹⁷ D. Stornaiuolo, S. Gariglio, A. Fete, M. Gabay, D. Li, D. Massarotti, and J.-M. Triscone, Physical Review B **90**, 235426 (2014).
- ¹⁸ J. Chen, H. Qin, F. Yang, J. Liu, T. Guan, F. Qu, G. Zhang, J. Shi, X. Xie, C. Yang, *et al.*, Physical Review Letters **105**, 176602 (2010).
- ¹⁹ T. Koga, J. Nitta, T. Akazaki, and H. Takayanagi, Physical review letters **89**, 046801 (2002).
- ²⁰ B. Burganov, C. Adamo, A. Mulder, M. Uchida, P. King, J. Harter, D. Shai, A. Gibbs, A. Mackenzie, R. Uecker,

- et al.*, Physical review letters **116**, 197003 (2016).
- ²¹ G. Cao, C. Alexander, S. McCall, J. Crow, and R. Guertin, Materials Science and Engineering: B **63**, 76 (1999).
- ²² Z. Qu, J. Peng, T. Liu, D. Fobes, L. Spinu, and Z. Mao, Physical Review B **80**, 115130 (2009).
- ²³ T.-H. Kao, H. Sakurai, S. Yu, H. Kato, N. Tsujii, and H.-D. Yang, Physical Review B **96**, 024402 (2017).
- ²⁴ N. Hollmann, Z. Hu, A. Maignan, A. Günther, L.-Y. Jang, A. Tanaka, H.-J. Lin, C. Chen, P. Thalmeier, and L. Tjeng, Physical Review B **87**, 155122 (2013).
- ²⁵ A. Krimmel, A. Günther, W. Kraetschmer, H. Dekinger, N. Büttgen, A. Loidl, S. Ebbinghaus, E.-W. Scheidt, and W. Scherer, Physical Review B **78**, 165126 (2008).
- ²⁶ T. Tran, K. Takubo, T. Mizokawa, W. Kobayashi, and I. Terasaki, Physical Review B **73**, 193105 (2006).
- ²⁷ D. Licciardello and D. Thouless, Physical Review Letters **35**, 1475 (1975).
- ²⁸ A. Ioffe and A. Regel, Prog. Semicond **4**, 237 (1960).
- ²⁹ A. Efros and B. I. Shklovskii, Journal of Physics C: Solid State Physics **8**, L49 (1975).
- ³⁰ N. F. Mott, Philosophical Magazine **19**, 835 (1969).
- ³¹ P. A. Lee and T. Ramakrishnan, Reviews of Modern Physics **57**, 287 (1985).
- ³² S. Hikami, A. I. Larkin, and Y. Nagaoka, Progress of Theoretical Physics **63**, 707 (1980).

Supplementary Material:
**Evidence for weak antilocalization-weak localization crossover and metal-insulator
transition in $\text{CaCu}_3\text{Ru}_4\text{O}_{12}$ thin films**

Subhadip Jana,^{1,2,*} Shwetha G.Bhat,³ B.C.Behera,¹ L.Patra,⁴ P.S.Anil Kumar,³ B.R.K.Nanda,⁴ and D.Samal^{1,2}

¹*Institute of Physics, Sachivalaya Marg, Bhubaneswar-751005, India*

²*Homi Bhabha National Institute, AnushaktiNagar, Mumbai-400085, India*

³*Department of Physics, Indian Institute of Science Bangalore-560012, India*

⁴*Condensed Matter Theory and Computational Lab,
Department of Physics, Indian Institute of Technology, Madras, India*

(Dated: December 8, 2020)

* subhadip.j@iopb.res.in

Different form of HLN equation

General expression for magneto-conductance(MC) (2D) was derived by Hikami,Larkin,Nagaoka which is known as HLN equation. The conductivity in presence of magnetic field (perpendicular to system's plane) given by [1]

$$\sigma(B) = \sigma_0 - \frac{e^2}{2\pi^2\hbar} \left(\psi(1/2 + 1/\tau a) - \psi(1/2 + 1/\tau_1 a) + \frac{1}{2}\psi(1/2 + 1/\tau_2 a) - \frac{1}{2}\psi(1/2 + 1/\tau_3 a) \right) \quad (1)$$

where $a = 4DeH/\hbar c$,

$$\frac{1}{\tau_1} = \frac{1}{\tau_{so}^i} + \frac{2}{\tau_s^i} + \frac{2}{\tau_s^i} + \frac{1}{\tau_e} - i\omega,$$

$$\frac{1}{\tau_2} = \frac{2}{\tau_s^i} + \frac{4}{\tau_s^i} + \frac{1}{\tau_e} - i\omega,$$

$$\frac{1}{\tau_3} = \frac{2}{\tau_s^i} + \frac{4}{\tau_{so}^i} + \frac{1}{\tau_e} - i\omega,$$

ψ is Digamma function, $\tau_{so}^i, \tau_s^i, \omega$ are scattering time due to i-th component contribution of spin-orbit interaction, localized magnetic interaction and omega related with the cutoff parameter respectively.

Impurity scattering amplitude can be written in general as

$$f_{\alpha\beta} = a\delta_{\alpha\beta} + ib(\vec{n} \times \vec{n}')\sigma_{\alpha\beta} + \vec{s}\sigma_{\alpha\beta}$$

where α, β are spin index of scattered electrons and \vec{n}, \vec{n}' are unite vector along the wave vectors before and after scattering \vec{k}, \vec{k}' respectively. a, b, \vec{s} are non-magnetic, spin-orbit and magnetic interaction amplitudes respectively.

$$\sigma_{\alpha\beta} = \langle \alpha | \sigma | \beta \rangle$$

σ is Pauli's matrices.

Over all scattering rate (Fermi-golden rule)

$$\frac{1}{\tau} = 2\pi\nu \sum_{\alpha, \gamma} \langle f_{\alpha\beta}(\vec{n}, \vec{n}') f_{\beta\gamma}(\vec{n}', \vec{n}) \rangle_{n'}$$

$$= \frac{1}{\tau_0} + \frac{3}{\tau_{so}} + \frac{3}{\tau_m}$$

where ν is density of scattering centers and $\tau_0, \tau_{so}, \tau_m$ are scattering time for non-magnetic, spin-orbit, magnetic interaction respectively.

Weak localization(WL) and Weak Anti localization(WAL) occurred by interference between two identical trajectory of scattered electrons. It is known as Cooperon loop. Impurity vortex pair can be written as

$$\Gamma = \langle f(\vec{n}, \vec{n}') \otimes f(-\vec{n}, -\vec{n}') \rangle$$

$$= \frac{1}{2\pi\nu\tau_0} - \frac{\sigma \otimes \sigma}{2\pi\nu\tau_{so}} + \frac{\sigma \otimes \sigma}{2\pi\nu\tau_m}$$

We introduce singlet(S), triplet(T) projection operators respectively

$$S = \frac{1 - \sigma \otimes \sigma}{4},$$

$$T = \frac{3 + \sigma \otimes \sigma}{4},$$

$$\Gamma = \frac{S}{2\pi\nu} \left(\frac{1}{\tau} - \frac{6}{\tau_m} \right) + \frac{T}{2\pi\nu} \left(\frac{1}{\tau} - \frac{1}{\tau_{so}} - \frac{2}{\tau_m} \right)$$

Vortex Γ are connected by pair of Green functions

$$\Pi(q) = \int \frac{(dq)^n}{(2\pi)^n} G^R(p+q) \otimes G^A(-p) \quad (\text{For } n \text{ dimension})$$

$$= 2\pi\nu\tau (1 - \tau Dq^2)$$

After taking summation over all maximally cross diagrams, the Cooperon propagator can be expressed as

$$C(q) = \frac{\Gamma}{(1 - \Pi\Gamma)}$$

$$= \frac{S}{2\pi\nu\tau^2} \left(Dq^2 + \frac{6}{\tau_m} \right)^{-1} + \frac{T}{2\pi\nu\tau^2} \left(Dq^2 + \frac{1}{\tau_{so}} + \frac{2}{\tau_m} \right)^{-1} \quad (2)$$

$$C(q) = \frac{\Gamma}{(1 - \Pi\Gamma)}$$

$$= \frac{S}{2\pi\nu\tau^2} \left(Dq^2 + \frac{6}{\tau_m} \right)^{-1} + \frac{T}{2\pi\nu\tau^2} \left(Dq^2 + \frac{4}{\tau_{so}} + \frac{2}{\tau_m} \right)^{-1}$$

Conductivity can be obtained by taking trace on spin indexes and integration over Cooperon loop with possible transferred momentum(q) during scattering for n-dimension

$$\Delta\sigma = -2e^2 \sum v_k^a v_{-k+q}^b (C(q)G^R(k)G^A(k)G^R(-k+q)G^A(-k+q))$$

$$= -\frac{2e^2\nu D\tau}{\hbar} \int \frac{(dq)^n}{(2\pi)^n} \text{Tr } C(q) \quad (3)$$

Using equation no (2) and trace over singlet and triplet give -1, 3 respectively conductivity becomes

$$\begin{aligned}\Delta\sigma &= -\frac{2e^2\nu D\tau}{\hbar} \int \frac{(dq)^n}{(2\pi)^n} \text{Tr} C(q) \\ &= \frac{e^2}{\pi\hbar} \int \frac{(dq)^n}{(2\pi)^n} [(q^2 + 6l_m^{-2})^{-1} - 3(q^2 + l_{so}^{-2} + 2l_m^{-2})^{-1}]\end{aligned}\quad (4)$$

For practical purpose, the integration limit of q has upper and lower cutoff. This can be approximated by considering simple case (i.e. absence of spin-orbit, magnetic scattering)

$$\int_{(D\tau_\phi)^{-1/2}}^{(D\tau_e)^{-1/2}} \frac{(dq)^2}{(2\pi)^2} \frac{1}{Dq^2} = \frac{1}{2\pi D} \ln(\tau_e/\tau_0) \quad (5)$$

where $L_{Th} = (D\tau_\phi)^{1/2}$, elastic length $l_e = (D\tau_e)^{1/2}$
Now we can rewrite equation(5) in a different way as given below

$$\begin{aligned}\int_{(D\tau_\phi)^{-1/2}}^{(D\tau_e)^{-1/2}} \frac{(dq)^2}{(2\pi)^2} \frac{1}{Dq^2} \\ = \int_0^\infty \frac{(dq)^2}{(2\pi)^2} \frac{1}{Dq^2 + (1/\tau_\phi)} - \int_0^\infty \frac{(dq)^2}{(2\pi)^2} \frac{1}{Dq^2 + (1/\tau_e)}\end{aligned}\quad (6)$$

Similarly the above equation can be written as given below in presence of other scattering process

$$\begin{aligned}\int_{(D\tau_\phi)^{-1/2}}^{(D\tau_e)^{-1/2}} \frac{(dq)^2}{(2\pi)^2} \frac{1}{q^2 + l_i^{-2}} \\ = \int_0^\infty \frac{(dq)^2}{(2\pi)^2} \frac{1}{q^2 + l_i^{-2} + l_{Th}^{-2}} - \int_0^\infty \frac{(dq)^2}{(2\pi)^2} \frac{1}{q^2 + l_i^{-2} + l_e^{-2}}\end{aligned}\quad (7)$$

In presence of magnetic field $\vec{q} \rightarrow \vec{q} + 2e\vec{A}$ where \vec{A} is magnetic vector potential.
Dynamics is quantized due to formation of Landau levels.

$$q_n^2 = (n + 1/2) \frac{4eB}{\hbar} \quad (\text{n is positive integer including zero}) \quad (8)$$

Complete expression of equation(4) regularized with cutoff parameters (for 2D)

$$\begin{aligned}\Delta\sigma &= \frac{e^2}{\pi\hbar} \int_0^\infty \frac{(dq)^2}{(2\pi)^2} ((q^2 + 6l_m^{-2} + l_{Th}^{-2})^{-1} - (q^2 + 6l_m^{-2} + l_e^{-2})^{-1}) \\ &+ \frac{3e^2}{\pi\hbar} \int_0^\infty \frac{(dq)^2}{(2\pi)^2} ((q^2 + l_{so}^{-2} + 2l_m^{-2} + l_e^{-2})^{-1} - (q^2 + l_{so}^{-2} + 2l_m^{-2} + l_{Th}^{-2})^{-1})\end{aligned}\quad (9)$$

In presence of magnetic field, the integration on q will be replaced by summation and substituting q_n value from equation(8) we get

$$\begin{aligned}\Delta\sigma &= \frac{e^2}{\pi\hbar} \sum_0^{n_{max}} \frac{(2\pi q_n dq_n)}{(2\pi)^2} ((q_n^2 + 6l_m^{-2} + l_{Th}^{-2})^{-1} - (q_n^2 + 6l_m^{-2} + l_e^{-2})^{-1}) \\ &+ \frac{3e^2}{\pi\hbar} \sum_0^{n_{max}} \frac{(2\pi q_n dq_n)}{(2\pi)^2} ((q_n^2 + l_{so}^{-2} + 2l_m^{-2} + l_e^{-2})^{-1} - (q_n^2 + l_{so}^{-2} + 2l_m^{-2} + l_{Th}^{-2})^{-1}) \\ &= \frac{e^2}{2\pi\hbar} \sum_0^{n_{max}} \frac{1}{l_B^2} \left(\left((n + \frac{1}{2})l_B^{-2} + 6l_m^{-2} + l_{Th}^{-2} \right)^{-1} - \left((n + \frac{1}{2})l_B^{-2} + 6l_m^{-2} + l_e^{-2} \right)^{-1} \right) \\ &+ \frac{3e^2}{2\pi\hbar} \sum_0^{n_{max}} \frac{1}{l_B^2} \left(\left((n + \frac{1}{2})l_B^{-2} + l_{so}^{-2} + 2l_m^{-2} + l_e^{-2} \right)^{-1} - \left((n + \frac{1}{2})l_B^{-2} + l_{so}^{-2} + 2l_m^{-2} + l_{Th}^{-2} \right)^{-1} \right)\end{aligned}\quad (10)$$

where $l_B = (\frac{\hbar}{4eB})^{1/2}$, n_{max} is highest Landau level quantum no

For simplicity we use some approximations

$$(q_n^2 + 6l_m^{-2} + l_e^{-2})^{-1} \simeq (q_n^2 + l_e^{-2})^{-1}$$

$$(q_n^2 + l_{so}^{-2} + 2l_m^{-2} + l_e^{-2})^{-1} \simeq (q_n^2 + l_e^{-2})^{-1}$$

To evaluate summation, we use identity of Digamma function $\psi(x) = \frac{\Gamma'(x)}{\Gamma(x)}$ where prime denote derivative.

$$\psi(x+n) = \psi(x) + \sum_{n=0}^{n-1} \frac{1}{x+n}$$

$$\sum_{n=0}^{n_{max}} \frac{1}{\frac{1}{2} + \frac{l_B^2}{l_i^2} + n_{max}} = \psi\left(\frac{1}{2} + \frac{l_B^2}{l_i^2} + n_{max} + 1\right) - \psi\left(\frac{1}{2} + \frac{l_B^2}{l_i^2}\right)$$
(11)

For good conductor, n_{max} is very large number. To find approximate value of $\psi\left(\frac{1}{2} + \frac{l_B^2}{l_i^2} + n_{max} + 1\right)$ we use an inequality

$$\ln(x) - \frac{1}{x} \leq \psi(x) \leq \ln(x) - \frac{1}{2x} \quad (\text{for } x > 0)$$

$$\lim_{x \rightarrow \infty} \ln(x) - \frac{1}{x} \leq \psi(x) \leq \ln(x) - \frac{1}{2x}$$

$$\simeq \ln(x) \leq \psi(x) \leq \ln(x)$$
(12)

Above inequality is only possible when

$$\lim_{x \rightarrow \infty} \psi(x) \rightarrow \ln(x)$$

using above results in equation (10) leads to

$$\Delta\sigma(B) = \frac{e^2}{\pi h} \sum_{n=0}^{n_{max}} \frac{1}{2} \left\{ \left(n + \frac{1}{2} \right) + \frac{6l_B^2}{l_m^2} + \frac{l_B^2}{l_{Th}^2} \right\}^{-1} + \left\{ \left(n + \frac{1}{2} \right) + \frac{l_B^2}{l_e^2} \right\}^{-1}$$

$$- \frac{e^2}{\pi h} \sum_{n=0}^{n_{max}} \frac{3}{2} \left\{ \left(n + \frac{1}{2} \right) + \frac{l_B^2}{l_{so}^2} + \frac{2l_B^2}{l_{Th}^2} \right\}^{-1}$$

$$= \frac{e^2}{\pi h} \left[-\frac{1}{2} \psi\left(\frac{1}{2} + \frac{6l_B^2}{l_m^2} + \frac{l_B^2}{l_{Th}^2}\right) + \frac{1}{2} \ln\left(\frac{6l_B^2}{l_m^2} + \frac{l_B^2}{l_{Th}^2}\right) - \psi\left(\frac{1}{2} + \frac{l_B^2}{l_e^2}\right) + \ln\left(\frac{l_B^2}{l_e^2}\right) \right.$$

$$\left. + \frac{3}{2} \psi\left(\frac{1}{2} + \frac{l_B^2}{l_{so}^2} + \frac{2l_B^2}{l_m^2} + \frac{l_B^2}{l_{Th}^2}\right) - \ln\left(\frac{4l_B^2}{l_m^2} + \frac{l_B^2}{l_{Th}^2}\right) \right]$$
(13)

For some system if magnetic moment scattering is negligible $l_m \rightarrow \infty$ i.e physically we can imagine that after traveling a very large distance, conducting electrons come across this type of scattering. With this approximation equation(13) becomes

$$\Delta\sigma(B) = \frac{e^2}{\pi h} \left[-\frac{1}{2} \psi\left(\frac{1}{2} + \frac{l_B^2}{l_{Th}^2}\right) + \frac{1}{2} \ln\left(\frac{l_B^2}{l_{Th}^2}\right) - \psi\left(\frac{1}{2} + \frac{l_B^2}{l_e^2}\right) + \ln\left(\frac{l_B^2}{l_e^2}\right) \right.$$

$$\left. + \frac{3}{2} \psi\left(\frac{1}{2} + \frac{l_B^2}{l_{so}^2} + \frac{l_B^2}{l_{Th}^2}\right) - \frac{3}{2} \ln\left(\frac{l_B^2}{l_{so}^2} + \frac{l_B^2}{l_{Th}^2}\right) \right]$$
(14)

Alternatively

$$\Delta\sigma(B) = -\frac{e^2}{2\pi^2 \hbar} \left[\psi\left(\frac{1}{2} + \frac{B_e}{B}\right) + \ln\left(\frac{B}{B_e}\right) + \frac{1}{2} \left\{ \psi\left(\frac{1}{2} + \frac{B_\phi}{B}\right) + \ln\left(\frac{B}{B_\phi}\right) \right\} \right.$$

$$\left. - \frac{3}{2} \left\{ \psi\left(\frac{1}{2} + \frac{B_{so} + B_\phi}{B}\right) + \ln\left(\frac{B}{B_{so} + B_\phi}\right) \right\} \right]$$
(15)

where $B_i = \frac{\hbar}{4el_i^2}$, $l_B = (\frac{\hbar}{4eB})^{1/2}$ and ϕ denotes phase de-coherent event by inelastic scattering which is identical with Thouless inelastic scattering in our discussion.

[1] S. Hikami, A. I. Larkin, and Y. Nagaoka, Progress of Theoretical Physics **63**, 707 (1980).